Journal of Alloys and Compounds 500 (2010) 16–21

Contents lists available at ScienceDirect

Journal of Alloys and Compounds

journal homepage: www.elsevier.com/locate/jallcom

Unusual electroresistive effect in ceramic $La_{0.49}Ca_{0.51}MnO_3$

K. Bärner[c,*], H. Deng[a], W. Morsakov[c], I.V. Medvedeva[b], C.P. Yang[a,*]

[a] Physics Department, Hubei University, Wuhan 430062, PR China
[b] Institute of Metal Physics, S. Kovalevskaya 18, 620219 Ekaterinburg, Russia
[c] Institute of Physics, University of Göttingen, F.Hund Platz 1, D-37077 Göttingen, FRG

ARTICLE INFO

Article history:
Received 10 December 2009
Received in revised form 24 March 2010
Accepted 31 March 2010
Available online 9 April 2010

Keywords:
Electroresistive effect
Phase separation
Natural spin transistor

ABSTRACT

The ER-effect in LCMO near the phase separation regime at $x = 0.48$ (Ca-content) is discussed in the framework of metallic/insulating layer sequences attached to internal boundaries. For $x = 0.51$, in particular, we find evidence for a natural spin transistor-like action based on the involvement of charge order stripe domains, which are characteristic for LCMO if $x > 0.5$.

1. Introduction

The electroresistive effect (ER) in manganites, although of high technological relevance, maintains to have some explanatory difficulties which mainly revolve around three questions,

(i) How to administer a high electrical field to the (sometimes metallic) samples?
(ii) How do internal and external boundaries influence the ER-effect?
(iii) Are the electronic–magnetic (EM) states of the manganites under a strong *E*-field different from those in the *E*-field free case?

The simplest situation would be provided by laser ablated manganite epitaxial layers, being single crystalline and having no internal surfaces. Note, however, that with the laser deposition, depending on the O_2-partial pressure in the deposition chamber, the total oxygen deficit of the sample is difficult to control and might change from charge to charge, even if the same base material is ablated.

Indeed, samples of $Nd_{0.7}Sr_{0.3}O_{3-\delta}$ grown epitaxially on $SrTiO_3$ behave differently [1]. A first sample, A_{6562} [1], having a maximal resistance at $T_{max} = 200$ K and a tentative δ of 0.02 does not show any ER-effect. That is different for sample C_{6568} ($\delta = 0.12$), which shows an ER-effect around a high resistance shoulder at 75 K.

For the epitaxial NSMO-layers made by another group [2], the dominant growth parameter is the decreasing O_2-partial pressure, too. Their sample A_4 has a T_{max} which matches that of A_{6562}, suggesting a similar oxygen content. The samples A_1–A_3 are probably even closer to stoichiometry. Note that they all develop a secondary maximum (T_{max}), while according to bulk data, the first relative maximum sitting on the right flank, represents the combined volume metal to insulator and Curie temperature $T_c = T_{mi}$.

The secondary maximum (T_{max}) has been assigned to the surface layers which are usually oxygen deficient beyond the bulk [3], mechanically stressed and under an internal electric field which stems from charged surface states (electrical stress).

All this now justifies to draw a space charge internal potential into the bulk of a ceramic sample [1], which can be modulated by an external field (electrical contact), so that the boundary resistance varies (one source of the ER-effect). Note, that with the epitaxial samples (first cell of the sequence viewed separately) the magnetic–electronic state at the surface must have changed under the mechanical and electrical stress, plus the oxygen deficiency, as evidenced by the large shift of T_{max}. The surface EM-state varies from that in the bulk, being either a coherent canted state, a frozen in phase separated state (both metastable), or a phase separated state with volume fractions changing with temperature T (near equilibrium state) [4–6] and always containing a large number of (oxygen deficit related) defects. Even if an epitaxial sample is close to stoichiometry, an insulating surface layer still exists, but it is rather narrow and contains less defects. Note further that the space charge fields only occur in the magnetically ordered state. If the boundary is far in the paramagnetic, hopping conductive state $T > T_{max}$, most of the trapped charges apparently take part in the conduction process, whereupon the electrical stresses disappear. At

* Corresponding authors.
E-mail addresses: k.baerner@t-online.de (K. Bärner), cpyang@hubu.edu.cn (C.P. Yang).

0925-8388/$ – see front matter © 2010 Elsevier B.V. All rights reserved.
doi:10.1016/j.jallcom.2010.03.232

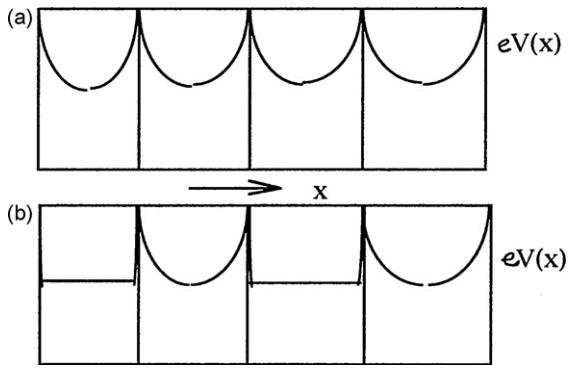

Fig. 1. (a) Grain boundary row of an insulating EM-phase; the line $eV(x)$ traces the conduction band edge. (b) Metal–insulator phase domain sequencing, yielding periodically extended back-to-back diode arrays. Horizontal line, Fermi level.

high temperatures we are then left with an inhomogeneous resistance. The same is true when the surface layer EM-state turns to metallic at low temperatures. The space charges will be increasingly screened, placing the maximal ER close to T_{max}, and leaving a large residual resistance. With our cited examples, all samples return to a more conductive state at low temperatures, except for C_{6568}, which remains all insulating.

The potential as drawn for the surface layer, periodically extended, yield a possible grain boundary potential sequence (Fig. 1). From that approach we can immediately draw two rules:

(1) One should find the exact replica's of the epitaxial layer resistance curves in oxygen deficient polycrystalline samples.
(2) Because of the larger number of (internal and insulating) boundaries in a polycrystalline sample, the ER-effect is enhanced as compared to a single epitaxial layer.

Both is found experimentally, A_1 corresponds to [6], A_4 and A_{6562} correspond to [7] and the ER-effect in oxygen deficient bulk NSMO is indeed very large as compared to that of comparable epitaxial layers [8,9]. For LCMO, the comparison of epitaxial layers [10,11] and ceramic samples [7,12] yields the same equivalency. There are, of course, exceptions from these rules if the parameter ranges of the interface layers cease to overlap; for example when the layer thickness gets very low (<150 nm), so that the nature of the connecting interfaces becomes the controlling factor.

If we can describe the ER-effect in polycrystalline samples that way, how about samples which by composition lie in a metallic/insulated phase separated region, like LCMO for $x = 0.48$ [13]. As shown in Fig. 1, while grain boundary sequencing yields a sequence of symmetric charged boundaries, M–I phase domain sequencing would yield rather a back-to-back diode sequencing, which should be different in its ER-response. Note, however, that because of the horizontal space charge boundaries, in both cases a sideways insulation exists between the different rows of grains, too.

In this contribution, we look if the ER-effect is enhanced in the case of M–I phase sequencing as compared to grain boundary sequencing and if it can be described quantitatively using the concepts introduced so far, plus Schottky barrier theory.

2. Experimental and results

With all the magnetic–electronic phase variants discussed so far, the lattice remains practically unchanged, probably due to the fact that the oxygen–oxygen (O–O) bonds provide the support structure of the manganite lattices. This is true for our ceramic LCMO sample with $x = 0.51$, as well. The lattice at room temperature is orthorhombic with parameters, $a = 0.5419$ nm, $b = 0.7641$ nm, and $c = 0.5429$ nm. The sample was made by conventional solid state reaction as described in detail elsewhere [14]. However, Fig. 2 shows an unusual ER-effect, (a) under constant current conditions and (b) under constant voltage conditions. The magnetization

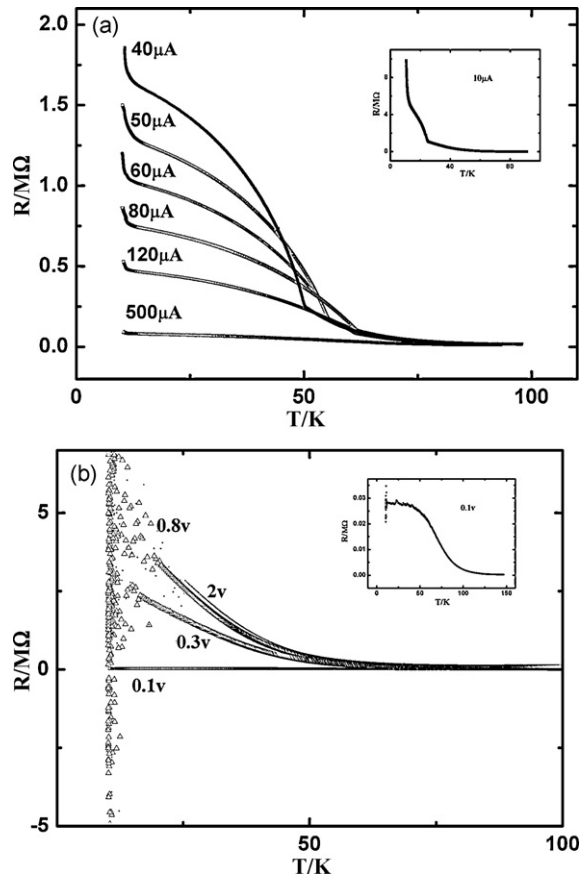

Fig. 2. Resistance versus temperature curves at constant current (a) and constant voltage (b) for the $x = 0.51$.

versus temperature curve $M(T)$ shows signs of magnetic heterogeneity, as expected. A metastability of the sample is indicated by (1) the absence of structure in the resistivity at the bulk magnetic ordering temperatures of LCMO with $x = 0.51$ [13]. On the other hand, (2), epitaxial samples of LCMO with x around 1/3 show a T_{max} around 100 K [11]. A third indication (3) is the unusual resistivity curve at low temperatures itself, which is similar to that of oxygen deficient epitaxial NSMO with $x = 0.3$, C_{6568} [1].

At this point we want to emphasize that thermal effects can be excluded to be significant in these experiments. First, it is hard to believe that an entropic force could create sharp structures as seen in Fig. 2a. Second, if we insert the Joule heat into the thermal current density over an arbitrary volume Δx^3 we arrive at $\Delta T = \Delta V^2/\rho\lambda$ for the temperature increase, with ρ: resistivity, λ: thermal conductivity, ΔV the voltage increment over a distance Δx. With a 1 μm grain size and 1 mm distance along the sample current, the sample applied potential of say 1 V drops over 10^3 barriers, i.e. 1 mV per barrier. Taking the other data from the literature [7], we obtain a 25 μK temperature change per barrier, which cannot nearly explain the ER-effects observed. Even if a single surface layer would be dominant, we would only have a 25 mK temperature change at the surface. Only using higher currents (20 V, 20 mA) we would arrive at 2.5 K, a value close to that reported for $Nd_{0.5}Ca_{0.5}Mn_{0.95}Ni_{0.05}O_3$ [15].

Fig. 2b shows some unusual "noise" in the constant voltage mode at low temperatures and high E-fields. Possibly, shallow traps get filled here, increasing the electrical field so much that cold emission takes place, reducing the electrical field again. This feedback mechanism would lead to fluctuating barrier potentials [14,16]. That would be an indication of very strong space charge electrical fields in LCMO at $x = 0.51$. If, accordingly, we assume short distance retrapping effects, that would provide a possibility to estimate the characteristic domain length L for $x = 0.51$: as we would have to assume almost ballistic transport, we may equate L with the mean free path $\lambda = v_F\tau$. The relaxation time τ can be obtained from the resistivity 1.2 mΩ cm (200 K), the carrier density, $n = 2 \times 10^{21}$ cm^3, both [17], the effective mass, $2.8m_o$, [18], and the Fermi energy, estimated between 2 and 4 eV. That data combined yields $\lambda = 15$–30 nm, which rather supports the existence of stripe domains dimensions rather than those of grain or phase domains, in which case the ER-effect would be rather unique, consistent with the size amendment of the rules 1 and 2.

Indeed, with the observation of charge order (CO) phase domains of 3–10 nm lateral extension in LCMO, only with $x > 0.5$ [14,19], such a scenario becomes even more plausible. Note, that Mn^{4+}/Mn^{3+} CO-domain sequencing would create excess

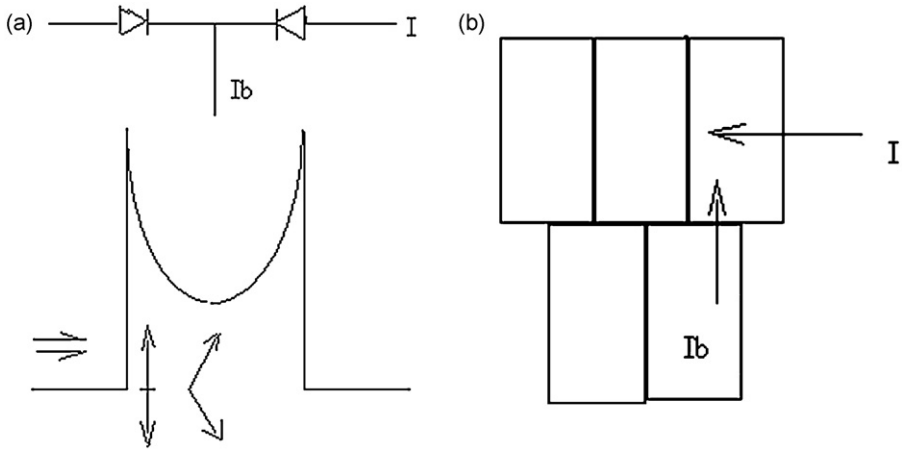

Fig. 3. (a) Space charge potentials and spin canting in x–z direction. In the figure the superlattice is reduced to one element, an insulating domain sandwiched between two metallic domains. (b) Two phase shifted internal boundary layer sequences; I: directed current, I_b: leakage current.

negative (Mn^{3+}) charges at the internal boundaries, probably creating even stronger fields [20] as those created by the (oxygen related) filled trap states at grain boundaries.

3. Discussion

First, we further narrow down the scenario elaborated in Section 1. Fig. 3a shows a single unit schematically, while in Fig. 3b we show two series of grains along the external current (or voltage) direction, electrically insulated against each other by vertical and horizontal grain boundaries [16], but phase shifted, so that because of potential differences between the centers and the edges of the grains—the external potential drops mainly at the boundaries—there can be a sideways leakage current I_b.

Assuming each second domain to be in a metastable ferromagnetic or canted metallic or semimetal state, while the other domains are insulating charge ordered antiferromagnetic, we would have here a back-to-back magnetic diode array like that of Fig. 1b.

3.1. Calculation of the I–V characteristic

First, assuming that without a magnetic field H, we have a non-magnetic Schottky barrier situation at each boundary, then, because of the barrier continuation, at least we have to discuss a pair of Schottky diodes wired in opposition. In that case, we are always in the reverse mode of one of the diodes and then the I–V characteristic would be:

$$I = I_0 \left(\exp\left(\frac{-e|V|}{kT} \right) - 1 \right) \tag{1}$$

where I_0, reverse saturation current; V, applied voltage, T temperature, e elementary charge, k Boltzman's constant, and I current. The maximal reverse (generation) current is [21]:

$$I_0 = \left(\frac{1}{6\pi} \right)^{(1/2)} (eN_c v_{th}) \exp\left(\frac{-W_a}{kT} \right) \tag{2}$$

for the case that the barrier width is small against the diffusion length [21]. N_c effective density of states at the conduction band, W_a metal/semiconductor work force, v_{th} thermal velocity. Note that Eq. (2) yields an exponential increase of $V/I = R(V \to 0) = kT/eI_0$ towards lower temperatures, as observed around 75 K (Fig. 2a), but there is no explicit dependence on I or V, i.e. no ER-effect.

Therefore, next we consider the case when the barrier width is large against the diffusion length. The reverse (space charge field dependent) current in this case has been written as [21]:

$$I_0 = e\mu_n E_R N_c \exp - \left(\frac{W_a}{kT} \right) \tag{3}$$

where μ_n the carrier mobility; E_R, space charge field at the boundary. Adding the external field E_{ext} portion to the space charge field of an individual boundary, $E = E_R + E_{ext}$, inserting E into Eq. (3) and I_0 into Eq. (1) we would obtain at least a voltage-ER-effect. Therefore, we differentiate Eq. (1) in order to extract a differential resistance R_D under consideration of Eq. (3). Specifically, if the reverse current I_0 depends on the electrical field at the boundary, an applied voltage V could further increase it. Writing the additional (small) current as a linear expansion term yields:

$$I_0 = I(V = 0) + i_0 = I(0) + cV \tag{4}$$

Here $I(0)$ is the space charge field determined current while i_0 is the excess current generated by the external electrical field. The proportionality factor c measures the voltage sensitivity. Now the differentiation of Eq. (1), with $dI/dV = 1/R_D$, yields:

$$\frac{1}{R_D} = (I_0 - I)\left(\frac{e}{kT} \right) + \frac{cI}{I_0}, \quad \text{for } I < I_0 \tag{5}$$

Note that when we turn to the differential resistance, we have given up to discuss the ER-effect globally. However, implicitly we assume that the field induced resistance change is a continuous function of the external field. Note further, that by not defining the field sensitivity factor c more closely, we leave room for a potential internal field amplification mechanism, which for example might be provided by the space charge repositioning mechanism that is discussed in [14].

Then, from Eq. (5) we obtain the limiting differential resistances at I, $V \to 0$ and at saturation $I \to I_0$ and $V \to V_e$. At this occasion we introduce the thermal voltage equivalent $kT/e = V_e$, which is the voltage where the reverse current saturation is practically reached (for example, $V_e = 30$ mV at room temperature).

$$\begin{array}{ll} \dfrac{1}{R_D} = \dfrac{I_0}{V_e} = \dfrac{I(0)}{V_e} & \text{for } I, V \to 0 \\ 1/R_D = c & \text{for } V \to V_e,\ I \to I_0 \end{array} \tag{6}$$

Note, that for obtaining an explicit dependence $R_D(V)$ from these two limiting values, we need an interpolation. As we already know that there has to be a curvature if the two end points are to have different tangents, we use a reduced third order polynominal for that interpolation:

$$\frac{V}{V_e} = v = \alpha i + \beta i^2 + \gamma i^3; \quad i = \frac{I}{I_0} \tag{7}$$

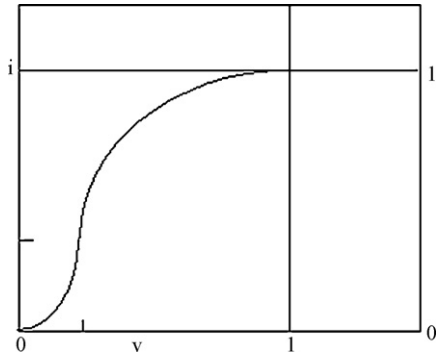

Fig. 4. Reduced i–v characteristic for an external field enhanced reverse current.

Asking for the two tangents to be observed and that $I(0)+cV_e$ is to be attained at V_e, we can determine the parameters α, β, γ. Making use of $I(0) \gg cV_e$, we obtain for the reduced v–i characteristic:

$$v = i - \beta i^2 + \beta i^3, \quad b = \left(\frac{I(0)}{cV_e}\right) - 1 \tag{8}$$

and by differentiation, dv/di, we obtain a reduced differential resistance $r(i)$:

$$\frac{R_D}{R_0} = r = 1 - 2\beta i + 3\beta i^2; \quad R_0 = \frac{V_e}{I_0} \tag{9}$$

Fig. 4 shows an example of the characteristic $i(v)$.

Note that while $r(i)$ is directly given by the derivative of $v(i)$ (Eq. (9)), in order to obtain $r(v)$, i has to be treated as a parameter variable. The second derivative shows that while the $r(i)$ minimum is at 1/3 on the i-scale, independent of β, the $r(v)$ minimum is at $1/3 - 2\beta/27$, i.e. β-dependent. The minimal resistances are equal and both dependent on β, $r(i)_{min} = 1 - \beta/3 = r(v)_{min}$. Because of the difference in the minima positions, defining an interval, both go down or up with i and v respectively outside that interval, while inside the interval $r(i)$ goes down and $r(v)$ goes up. The absolute resistance $R = V/I$ cannot be simply obtained globally from the integration of the differential resistance, but locally if one uses the almost linear in parts nature of $r(i)$ and $r(v)$ as depicted in Fig. 5. In Fig. 5 the slope changes from negative to positive at the minima, passing zero in a very small interval only. Furthermore, as $r = 1$ ($\beta = 0$) represents an ohmic resistance (zero ER-effect),

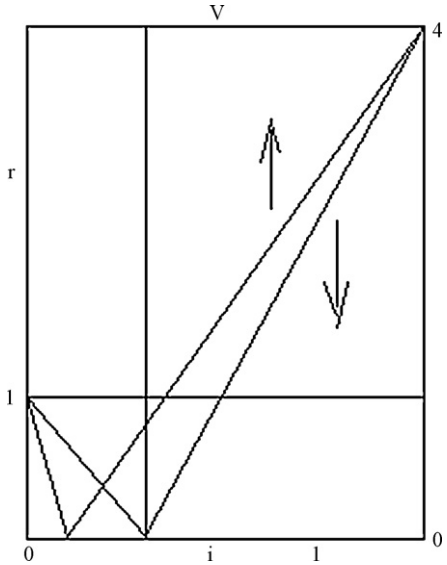

Fig. 5. The minimum of $r(i)$ is always at 1/3, while that of $r(v)$ depends on β; both touch zero for $\beta = 3$.

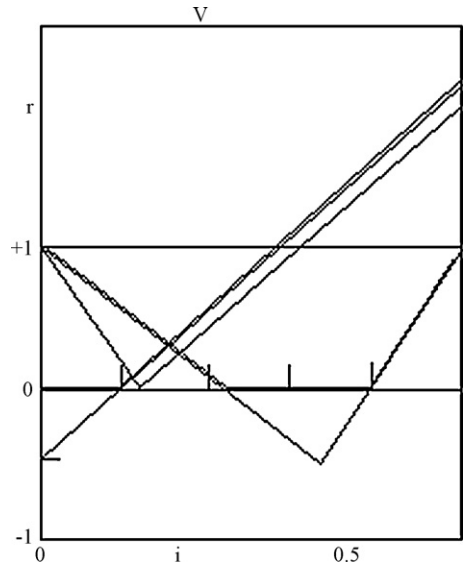

Fig. 6. The differential resistance develops zero ER-intervals if $4.5 < \beta < 3$. This can lead to fixpoints in the $R(I,T)$ or $R(V,T)$-curves.

the resistance differences $\Delta r(v) = r - 1 = \varepsilon v$ and $\Delta r(i) = \delta i$ determine the respective voltage- and current-ER effects. Integrating $\Delta r(i)$ between two close current values, i_1 and i_2, yields:

$$\Delta r_{21}(i) = \delta i_a; \quad i_a = \frac{i_1 + i_2}{2}; \quad i < 1/3 \tag{10}$$

Equivalently,

$$\Delta r_{21}(v) = \varepsilon v_a, \quad v_a = \frac{v_1 + v_2}{2}; \quad v < v_{min} \tag{11}$$

Recalling that $r = R_D/R_0$, $I = I/I_0$ and $v = V/V_e$ allows to compare Eqs. (10) and (11) with the experimental resistance increments. Similar equations exist also for the ascending slopes; here $\Delta r(v) = r - 1 = \beta + \varepsilon'(1 - v)$ and $\Delta r(i) = \beta + \delta'(1 - i)$. Note, that the slopes are inverted in respect to those of Eqs. (10) and (11), as expected (see Fig. 5).

If at the minima, the $r(i)$ or $r(v)$ curves change slope, the differential resistance is zero, i.e. we have a local fix point, i.e. a point where at least two of the $r(i)$ (or $r(v)$) curves cross, as $\Delta r_{21} = 0$ when δ or $\varepsilon = 0$. For $\beta = 3$ the minima touch the abscissa, $r = 0$. Going with the minima to negative values, other unusual features are obtained. For $r(i)$ for example, with the β-parameter increasing beyond 3 one would find negative r-values around $i = 1/3$ (Fig. 6). Note, however, that there are no negative differential resistances in the original i–v characteristic (Fig. 4), suggesting that the negative values have to be replaced by $r = 0$. Then, the slopes ε and δ are zero in a whole current or voltage region and there the spread of curves, i.e. the ER-effect vanishes (global fix point). The parameter range of β closes at $\beta = 4.5$, as v_{min} cannot go below zero. Therefore, we should observe also a maximal ascending slope (Fig. 6), i.e. a saturation of the voltage-ER.

3.2. ER-effect in $x = 0.51$—comparison with the experiment

For $x = 0.51$, with L much shorter, at first sight we would expect to be in the generation current regime, i.e. to observe no ER-effect. However, we find both a significant current-ER and voltage-ER, suggesting that the internal E-fields are important here, too.

Next, as the voltage per barrier at 25 K is about 0.004 in the relative v-scale, we expect the voltage increment ΔR_{21} to go down with increasing V_a. Indeed, the voltage increment goes down, approaching zero between 0.8 and 2 V, suggesting that we are close to a fix point at the abscissa. The current increment we would expect

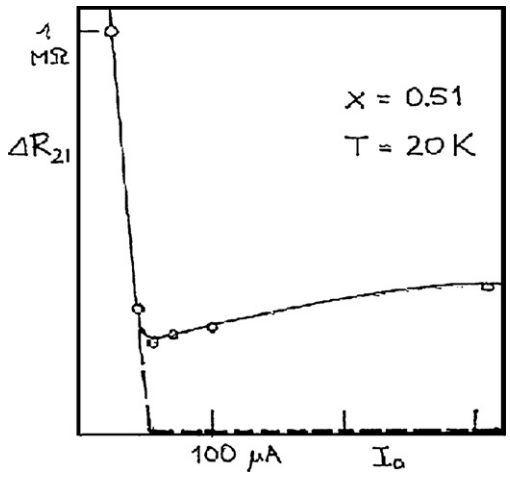

Fig. 7. Current resistance increment ΔR_{21} versus average current for $x = 0.51$ at 20 K. Points: experimental data sample 1 (Fig. 4a). Dashed line: calculation.

to go down, too, and initially it does so, but then it goes up again (Fig. 7). The data points are collected from two different $x = 0.51$ samples. The large shifts observed along the $r(i)$ or $r(v)$ lines under quite moderate external voltages suggest again an effective voltage amplification mechanism. The voltage increment (Fig. 2b) suggests that in particular $\beta > 3$, but the current increment indicates that at the resulting fix point (interval), where we expect to loose the ER-branching, another process takes over. Note, that in that particular regime of current-ER we observe pairwise crossing over, with all curves finally merging at higher temperatures (Fig. 2). At the pairwise crossing points obviously the current increment ΔR_{21} is zero, so that these temperatures qualify as local fix points. The spread of these points followed by the final merger confirms that a global fix point did exist. Thus, while likely $4.5 > \beta > 3$ for $x = 0.51$, there exist both current and temperature intervals, where instead of a zero current-ER, another process, one which delivers a finite current-ER effect, takes over.

3.3. Temperature dependence of the boundary differential resistance $R_D(T)$

As we suspect the $R(T)$ curvature to be significant, we now look at the differential boundary resistance versus temperature curve $R_D(T)$. If $R_D(T)$ needs to be calculated, in principle one has to know $R_0(T)$ and $\beta(T)$. While β is restricted, $0 < \beta < 4.5$, $R_0 = V_e/I_0$ should rise with lowering T. As we suspect $\beta > 3$ for $x = 0.51$ at least for a certain temperature interval, we start the calculation around the minimal resistance R_m versus temperature curve in the current mode. Then, from $R_m(T)/R_0 = 1 - \beta/3$ we obtain:

$$R_m(T) = \left(\frac{V_e}{I_0}\right)\left(\frac{(4/3) - (1/3)I(0)}{cV_e}\right); \quad I_0 = I(0) + cV_e \tag{12}$$

Note, that after multiplication, the first term is inversely proportional to $I(0) = I_{00}\exp(-W/kT)$ (Eq. (1)) while with the second term $I(0)$ almost cancels. Extracting $I(0)$ and using the expansion $1/(1+x) = 1 - x + \ldots$, based on $I(0) \gg cV_e$, we obtain a parabolic equation:

$$R_m = \left(\frac{1}{3c}\right)(Ay - By^2 - 1), \quad A = \frac{5cV_e}{I_{00}}; \; B = \frac{4(cV_e)^2}{I_{00}^2} \tag{13}$$

with $y = \exp(+W/kT)$ as the major temperature dependence involved. The zero points are then $y_1 = I_{00}/cV_e$ and $y_2 = (1/4)I_{00}/(cV_e)$, indicating that $R_m < 0$ in between these two solutions, which means that we have to replace R_m with $R_m = 0$ inside the temperature interval opened by $(y_1 - y_2)$. Obviously,

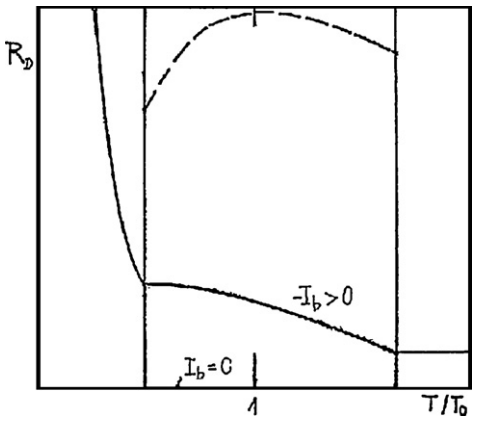

Fig. 8. Reconstruction of the $R_D(T)$-curve from the three sections, including an interval matching procedure. Parameters for $I_b > 0$; $w = W$, $I_{00}/cV_e = 7.3$.

the zero point of $R_m(I)$ expands into a temperature interval, in which the current ΔR-increment is zero. This result suggests also that we may get a fair approximation of $R_D(T)$ by approximating for the outside intervals in a global way, too. Specifically, we use $R_L = R_D(i = 0)$ for $y > y_1$ (the lower temperatures) and $R_R = R_D(i = 1)$ for $y < y_2$ (the higher temperatures). Since:

$$R_L = R_0 = \frac{V_e}{I(0)} \tag{14}$$

and

$$R_R = \frac{V_e I(0) + cV_e}{cV_e I(0)} \approx \frac{1}{c} \tag{15}$$

both R_L and R_R are independent of β. Combined, we already have a composite solution for $R_D(T)$ which is shown by example in Fig. 8. The left interval of Fig. 7 holds an exponential function increasing with lowering T, the right interval is a constant and for the middle interval R_D is zero. Note, that if $R_D = 0$ in the middle interval, in this approximation we would have no ER-effect at medium temperatures. The zero crossings $y_{1,2}$, however, apparently have some relation to the two temperatures where the curvature of the experimental $R(T)$ changes from negative to positive (or zero).

Probably the missing element is the leakage current I_b. In this context note, that if the distance between the back to back diode boundaries gets small, like with $x = 0.51$, we may expect some kind of transistor action, i.e. an interference between a collector and an emitter current provoked by a base current. Here, if we simply add a side current I_b to $I(0)$, in the left hand interval we get a boundary differential resistance which decreases with increasing I_b – assuming that I_b is in the end generated by the outside current source, too – while for the right hand interval we still get a constant value. The resistance of both outside parts is still ER-spliced, but now for the middle section we expect an ER-splicing, too. The argument goes in detail as follows:

After adding I_b to $I(0)$, and staying close to the minimum condition without I_b, i.e. at $y = (1/4)(I_{00}/cV_e)$, $R_m(T)$ takes the following form:

$$R_m(T) = \frac{V_e}{I_0}\left(-\frac{I_b}{cV_e}\right); \quad I_0 = I(0) + cV_e + I_b; \; V_e = \frac{kT}{e} \tag{16}$$

consistent in sign with the result for $I_b = 0$. I_b, however, can change sign once the base regions get (differentially perfect) conducting. In that case, the second bracket would become positive and it would dominate the middle region, with I_b increasing the resistance, as indeed observed initially – compare $R(T)$ of 10 μA and 40 μA [1]. Adding I_b to $I(0)$, one also has an effect on the extension of the zero interval: with I_b not changing sign, the interval would narrow as the solutions $y_{1,2}$ come closer to each other with increasing I_b.

However, if we hold on to the argument that I_b does change sign at $y_{1,2}$, then $I_b = 0$ at $y_{1,2}$, and the zero interval extension would not change. Indeed, experimentally y_1 changes insignificantly to the left and y_2 a little stronger to the right, increasing the interval, but not significantly (see Fig. 2).

With leakage currents existing, apparently the global fix point property of the interval gets lost, while some local signatures remain.

Fig. 8 also shows $R_D(T)$, now at $I_b > 0$. The curvature in the new middle section we assign to a (weaker) activated behaviour of I_b, $I_b = I_{b0}\exp(-w/kT)$ with $w \leq W$, yielding the function $(1/T)\exp(-T_0/T)$ for the second bracket, which indeed exhibits a negative curvature around its maximum, which may well lie in the middle temperature region.

Combining the results obtained in the three intervals can now be done simply by matching the differential resistances at the two connecting points. Note that because of the factorisation of $R_D(T)$, first the factor given by the exponential and the constant value have to be considered. They have to be multiplied with the middle section edge points, respectively, with a linear interpolation in between. Thereafter the edge resistances have to be matched, again by two different factors, again the factors linearly interpolated in between. The end result is depicted in Fig. 8. While we do not measure the differential resistance directly, we can now understand the source of the negative curvature, the dilution of the fix points at $y_{1,2}$, as well as the ER-effect at all temperatures.

So far, no magnetic field has been used systematically on the compound with $x = 0.51$. However, the ER-effects in CMR-materials are often found intertwined with the MR-effects [8,9] and this can be viewed as argument that a spin property will be involved here, too. Preliminary measurements under external magnetic fields yield a small MR, for example $\leq 11.5\%/T$ at 32.5 K [22].

4. Conclusions

Electrically active boundary sequences in some high resistive CMR-materials can be described by Schottky barrier back-to-back diodes in the reverse electrical field dependent current mode, likely including a field sensitivity enhancing charged trap state relocation mechanism. For $La_{0.49}Ca_{0.51}MnO_3$ in particular, because of the existence of charge order stripe domains, the barriers come that close to each other that a natural transistor action can be observed.

Acknowledgments

The authors thank the Natural Science Foundation of China (Grant Nos. 10774040 and 10911120055), the Program for New Century Excellent Talents in University and the Alexander von Humboldt Foundation for their support.

References

[1] W. Morsakov, Electroresistive effect in Sauerstoffdefizitärem manganite $Nd_{2/3}Sr_{1/3}O_{3-\delta}$, thesis, Gòttingen, 2006.
[2] W. Schnelle, A. Poddar, P. Muruguraj, E. Gmelin, R.K. Kremer, K. Sasaki, J. Maier, J. Phys. C 12 (2000) 4401–4416.
[3] I. El-Kassab, A.M. Ahmed, P. Mandal, K. Baerner, A. Kattwinkel, U. Sondermann, Physica B 305 (2001) 233–241.
[4] K. Bärner (Ed.), New Trends in the Characterization of CMR-manganites and Related Materials, Research Signpost, ISBN 81-308-0043-8, 2005, p. 1ff.
[5] K. Bärner (Ed.), Double Exchange in Heusler Alloys and Related Materials, Research Signpost, ISBN 81-308-0152-3, 2007, p. 1ff.
[6] K. Bärner, W. Morsakov, I.V. Medvedeva, H. Deng, C.P. Yang, Physica B 404 (2009) 11–15.
[7] J. Liebe, H. Kang, L. Haupt, P. Mandal, I.V. Medvedeva, G.H. Rao, K. Bärner, A. Poddar, P. Muruguraj, R. Fischer, E. Gmelin, E. Gommert, R.v. Helmolt, J. Wecker, J. Appl. Phys. 83 (1998) 7148–7150.
[8] C.P. Yang, V. Morchshakov, I.O. Troyanchuk, G.H. Rao, K. Bärner, J. Alloys Compd. 383 (2004) 45–48.
[9] C.P. Yang, S.S. Chen, Z.H. Zhou, L.F. Xu, H. Wang, J.F. Hu, V. Morchshakov, K. Bärner, J. Appl. Phys. 101 (2007), 063909-1–063909-4.
[10] R.v. Helmolt, Fortschrittberichte, VDI Duesseldorf, 1995, p. 5/412.
[11] J. Liebe, E. Kraus, L. Haupt, P. Mandal, K. Bärner, Appl. Phys. Lett. 68 (17) (1996) 2343–2345.
[12] R.v. Helmolt, L. Haupt, Ch. Zock, K. Bärner, Proceedings of the International Symposium on Superconductivity and Tunneling Phenomena, Slavjanogorsk, Ukraine, September 21–25, 1992, 1992, p. 102.
[13] P. Schiffer, A. Ramirez, W. Bao, S.W. Cheong, Phys. Rev. Lett. 75 (18) (1995) 3336–3339.
[14] K. Bärner, H. Deng, H. Wang, M. Annaorazov, I.V. Medvedeva, C.P. Yang, Physica B 10 (2009) 041, in press.
[15] A. Rebello, R. Mahendiran, Solid State Commun. 149 (17–18) (2009) 673.
[16] V. Morchshakov, M.P. Annaorazov, H.S. Aybar, C.P. Yang, I.O. Troyanchuk, K. Bärner, J. Appl. Phys. 105 (2009), 063704-1–063704-7.
[17] A. Poddar, P. Muruguraj, E. Fischer, K. Bärner, L. Haupt, P. Mandal, G.H. Rao, Physica B 254 (1998) 21–27.
[18] J.R. Simpson, H.D. Drew, V.N. Smolyaninova, R.L. Greene, M.C. Robson, A. Biwas, M. Rajeswari, Phys. Rev. B 60 (1999) R16263–R16266.
[19] S. Mori, C.H. Chen, S.W. Cheong, Letters to Nature 392 (1998) 473–476.
[20] A. Asamitsu, T. Tomioka, H. Kuwahara, Y. Tokura, Nature 388 (1997) 50–52.
[21] E. Spenke, Elektronische Halbleiter, Springer, NY, 1965, pp. 130–132.
[22] H. Deng, C.P. Yang, Z.H. Zhou, H. Wang, K. Baerner, I.V. Medvedeva, J. Phys. Chem. Solids, in press only during the proof-reading., 2010, submitted.